Title

Response to Extreme Temperatures of Mesoporous Silica MCM-41: Porous Structure Transformation Simulation and Modification of Gas Adsorption Properties

Journal

Langmuir, 32(44)

ISSN

0743-7463

Authors

Zhang, Shenli
Perez-Page, Maria
Guan, Kelly
et al.

Publication Date

2016-11-08

DOI

10.1021/acs.langmuir.6b02814

Peer reviewed

LANGMUIR

Article

pubs.acs.org/Langmuir

Response to Extreme Temperatures of Mesoporous Silica MCM-41: Porous Structure Transformation Simulation and Modification of Gas Adsorption Properties

Shenli Zhang,[†,‡] Maria Perez-Page,[†,‡] Kelly Guan,[†,‡] Erick Yu,[†,‡] Joseph Tringe,[§] Ricardo H. R. Castro,[‡] Roland Faller,[*,†] and Pieter Stroeve[*,†]

[†]Department of Chemical Engineering and [‡]Department of Materials Science and Engineering, University of California—Davis, Davis, California 95616, United States

[§]Lawrence Livermore Laboratory, Livermore, California 94550, United States

Supporting Information

ABSTRACT: Molecular dynamics (MD) and Monte Carlo (MC) simulations were applied together for the first time to reveal the porous structure transformation mechanisms of mesoporous silica MCM-41 subjected to temperatures up to 2885 K. Silica was experimentally characterized to inform the models and enable prediction of changes in gas adsorption/separation properties. MD simulations suggest that the pore closure process is activated by a collective diffusion of matrix atoms into the porous region, accompanied by bond reformation at the surface. Degradation is kinetically limited, such that complete pore closure is postponed at high heating rates. We experimentally observe decreased gas adsorption with increasing temperature in mesoporous silica heated at fixed rates, due to pore closure and structural degradation consistent with simulation predictions. Applying the Kissinger equation, we find a strong correlation between the simulated pore collapse temperatures and the experimental values which implies an activation energy of 416 ± 17 kJ/mol for pore closure. MC simulations give the adsorption and selectivity for thermally treated MCM-41, for N_2, Ar, Kr, and Xe at room temperature within the 1−10 000 kPa pressure range. Relative to pristine MCM-41, we observe that increased surface roughness due to decreasing pore size amplifies the difference of the absolute adsorption amount differently for different adsorbate molecules. In particular, we find that adsorption of strongly interacting molecules can be enhanced in the low-pressure region while adsorption of weakly interacting molecules is inhibited. This then results in higher selectivity in binary mixture adsorption in mesoporous silica.

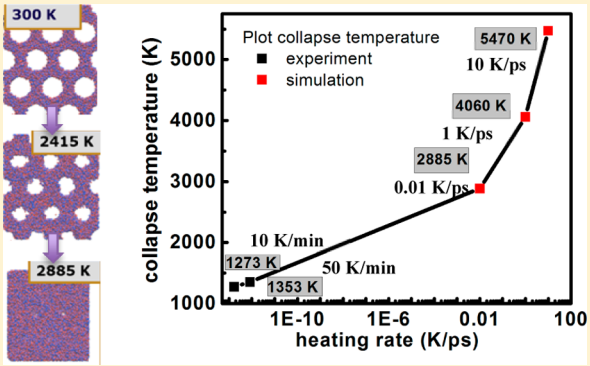

1. INTRODUCTION

There is an increasing need to capture and treat harmful gases from vehicles and industrial processes to prevent environmental contamination and degradation. Particularly relevant to this study, fission reactions in nuclear power plants and fuel rod reprocessing can generate and release radioactive noble gases. Insights developed for noble gases can be applied more broadly to include other molecules of interest. For direct implementation of porous materials into all these scenarios, a good understanding of, not only the gas adsorption properties, but also the materials behavior upon heating is required, since sorption and catalytic properties can be altered in the dehydrated/calcined state at relatively high operation temperatures. Materials with excellent adsorption properties and thermal stability are considered to be promising candidates, such as zeolites, porous silica and materials from the carbide family.[1,2] Mesoporous silica MCM-41, which is characterized by a hexagonal arrangement of uniform pores with the diameter tunable from 1.5 to 10 nm,[3] was chosen for study here because of its high specific surface area (>1000 m^2/g) and good thermal and hydrothermal stability (~900 °C).[3−5]

Morphology and surface area changes in MCM-41 upon heating have been studied experimentally.[4,6] The porous structure decreases continually with temperature until a complete collapse of the porous structure occurs. However, the fundamental structural evolution mechanism of MCM-41 during heating is not yet understood because the microscopic structural changes such as the roughness of the pore surface is difficult to characterize and the influence on the materials adsorption is not known in detail. Simulations are useful to identify these factors and explain experimental observations. Various MCM-41 models with different microscopic details have been proposed for gas adsorption studies using Grand Canonical Monte Carlo.[7−11] In Maddox et al.,[7] MCM-41

Received: July 28, 2016
Revised: October 5, 2016
Published: October 17, 2016

DOI: 10.1021/acs.langmuir.6b02814
Langmuir 2016, 32, 11422−11431

models with different surface energy contours were compared and it was shown that surface heterogeneity influences the gas adsorption isotherms as well as the hysteresis during gas desorption. He and Seaton[8] generated three MCM-41 models with different surface roughness values: one smooth with homogeneous cylindrical pores, and two other heterogeneous structures generated by forming pores into both crystal and amorphous silica phases. Other methods that can imitate the real sol−gel synthesis process have also been proposed to generate more realistic pore surfaces;[9,10] including the introduction of surface hydroxyl groups for a more accurate chemical description when adsorption of polar molecules, such as water, is considered.[11] MCM-41 models that undergo thermal treatment have not been generated nor discussed. A common difficulty in heating simulations is superheating: the extremely fast heating rates required for computer simulations are incommensurate with experimental heating rates. This can lead to simulations producing unrealistic melting points and other phase transition temperatures.[12]

The capture of different gases by MCM-41 has been widely studied in both experimental and simulation studies, including N_2,[13] noble gases,[9,10] CO_2,[8,11] and alkanes.[8] The application to adsorption and storage of noble gases is very important during nuclear power operations and waste treatment.[14,15] The simple force field description of noble gases makes them suitable to test and verify adsorption theory and simulation models.[9,10,16] Previous studies focused on cryogenic temperatures where adsorption occurs most effectively. Due to the high cost of refrigeration and the practical relevance of in situ gas storage, it is important to understand noble gas adsorption and storage behavior at higher temperatures over a wide range of pressures. Another related issue is the selectivity for different noble gases. Although MCM-41's separation properties have been investigated at cryogenic or room temperature for a few gases,[8,11] detailed knowledge of high-temperature high-pressure adsorption/separation behavior of noble gases in MCM-41, including the influence of thermal treatment on this adsorption material, is still needed.

Here, molecular dynamics (MD) and Monte Carlo (MC) simulations are implemented along with experiments to investigate, for the first time, the porous structure transformation mechanism and modification of gas adsorption/separation properties at temperatures up to 2885 K. To inform the model with realistic material parameters, MCM-41 samples are synthesized and experimentally characterized with XRD, TG/DSC and pore size distributions. The pore closure activation energy can link the simulation time scale to the experimental scale, allowing for a robust understanding of the process. Next, the Grand Canonical Monte Carlo method is used to predict the adsorption behavior of N_2, Ar, Kr and Xe at 300 K for pressures from 1 to 10 000 kPa. Untreated MCM-41 and a thermally degraded MCM-41 are selected to study the modification of the adsorption properties due to thermal treatment. The materials are analyzed by determining the absolute and excess adsorption isotherms, the surface roughness and the radial density profile. Finally, the adsorption of Kr/Ar and Kr/Xe are simulated to determine the change in selectivity.

2. METHODOLOGY

2.1. Simulation. *2.1.1. Construction of Untreated MCM-41 Model.* The MCM-41 structure is generated by molecular dynamics using the LAMMPS package.[17] A rectangular unit cell with one pore at the center and a quarter pore at each corner is chosen to represent the hexagonal pore arrangement in MCM-41 (Figure 1). The center-to-center distance between two pores is obtained from XRD experiments; the pore diameter is based on the pore-size distribution obtained from N_2 gas adsorption. Periodic boundary conditions are applied in x, y, and z directions.

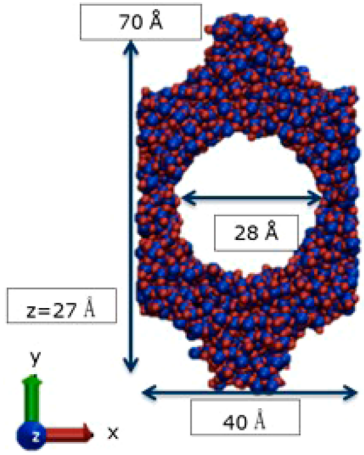

Figure 1. Simulation cell of the MCM-41 structure. Colors for atoms: blue is silicon; red is oxygen.

The bulk amorphous silica phase was first constructed using a random-insertion process.[8] Si and O atoms are randomly inserted into a simulation box such that (1) the ratio of silicon and oxygen atoms is 1:2 and (2) a total of 962 SiO_2 units are inserted to reach a density of 2.2 g/cm^3 in a box of 40 Å × 70 Å × 27 Å. Silicon atoms were inserted first such that no two Si are within 3 Å from each other. Oxygen atoms were then placed at least 1.85 Å away from other atoms. The structure was then melt-quenched under NVT condition using a Tersoff potential[18,19] to generate amorphous silica. T was increased from 300 to 3300 K by 10 K/ps and then quenched down at 1 K/ps. The system was equilibrated at 300 K for 50 ps. Pores were created by deleting atoms in a cylindrical region of d = 28 Å (and d = 31 Å). Finally, the silicon to oxygen ratio was checked and 18 oxygen atoms were randomly inserted into the silica matrix to ensure a Si/O of 1:2. The final structure is equilibrated at 300 K first under NVT and then under NPT condition (P = 1 bar) for 10 ns each. This MCM-41 structure is referred to as the "300 K MCM-41 model".

2.1.2. Thermal Stability Study. Thermal stability of the as-built MCM-41 structure with d = 28 Å was studied using NPT (P = 1 bar). The temperature of the amorphous cell (replicated 3 × 2 × 2 in the x, y, and z directions of the 300 K MCM-41 unit cell) was continuously increased from 300 to 5000 K to observe the continuous structure evolution at heating rates of 10, 1, and 0.01 K/ps. Using the slowest heating rate (0.01 K/ps), structures at several temperatures (1273, 1773, 2180, 2415 K, 2650 and 2885 K) are sampled. For this, the original 300 K MCM-41 unit cell (here replicated twice in the z direction) was heated to the designated temperature (referred to as the heating process), then the temperature was kept constant for 20 ns (referred to as the hold stage), and then cooled back to 300 at 0.01 K/ps and equilibrated for 1 ns. These structures are referred to as the "1273 K (or 1773, 2180, 2415, 2650 K, or 2885 K) MCM-41 model". Due to the nature of amorphous material, the metastable state is tightly linked with the initial conditions, so the exact heated structure cannot be fully reproduced if initial velocities and positions are different. Therefore, three independent samples were generated for each temperature. Samples 1 and 2 were generated from two independent 300 K MCM-41 structures. Samples 2 and 3 were from the same 300 K structure, but with different initial velocities for the heat treatment.

2.1.3. Gas Adsorption Simulation. We used Grand Canonical Monte Carlo (GCMC) as implemented in the MCCCS Towhee

DOI: 10.1021/acs.langmuir.6b02814
Langmuir 2016, 32, 11422−11431

code[20] to characterize adsorption properties of the above models. First, we obtained the chemical potential as a function of pressure of different gases at relevant temperatures using particle insertion. The adsorbent was then introduced and the matrix was fixed during the Monte Carlo simulation. We used a 9-6 Lennard−Jones-like potential truncated at 10 Å and the sixth power mixing rule[21] to describe the adsorbate−adsorbate and adsorbate−adsorbent interactions.

$$\varphi(r)_{9\text{-}6} = 6.75\epsilon\left[\left(\frac{\sigma}{r}\right)^9 - \left(\frac{\sigma}{r}\right)^6\right] \quad (1)$$

$$\sigma_{ab} = \left(\frac{{\sigma_{aa}}^6 + {\sigma_{bb}}^6}{2}\right)^{1/6} \quad (2)$$

$$\varepsilon_{ab} = (\varepsilon_{aa}\varepsilon_{bb})^{1/2}\frac{2{\sigma_{aa}}^3{\sigma_{bb}}^3}{{\sigma_{aa}}^6 + {\sigma_{bb}}^6} \quad (3)$$

Only the oxygen atoms in the adsorbent interact. Silicon atoms are ignored since their low polarizability results in a negligible dispersion interaction.[22] The parameters employed in our simulation are listed in Table 1. Oxygen parameters are optimized against experimental nitrogen adsorption at 77 K by comparing the adsorption amount at low pressure, saturated adsorption amount and condensation pressure (ε is varied with energy step of 20 K and σ with step of 0.2 Å). Other simulation parameters are from the COMPASSv1 force field.[23] The data are collected after 5×10^7 Monte Carlo steps for equilibration.

Table 1. Lennard−Jones 9-6 Parameters for Oxygen in a Silica Matrix and Various Gas Molecules[a]

	ε (K)	σ (Å)
O−O	75	3.44
N−N	30.09	3.8008
Ar−Ar	100.64	3.88
Kr−Kr	140.9	4.3
Xe−Xe	196.25	4.26

[a]Only the parameters of oxygen have been optimized against experimental values; the parameters for other gas molecules were obtained from COMPASSV1 force field implemented in MCCCS Towhee.

2.2. Experimental Section. *2.2.1. Synthesis of MCM-41 Mesoporous Silica Nanoparticles.* We used the sol−gel method to produce MCM-41 type MSNs.[3] In a typical process, a surfactant such as hexadecyl trimethylammonium bromide (CTAB) is used to form micelles, which serve as template for the mesoporous silica nanoparticles. Next a silica source such as tetraethyl orthosilicate (TEOS) is introduced under aqueous, basic conditions, resulting in the hydrolysis of silicate and formation of a silica network around the template. To produce MCM-41, 500 mg of CTAB was initially dissolved in 240 mL of 0.014 M NaOH. The solution was stirred and the CTAB was added slowly. The solution was then heated to 80 °C and 2.5 mL of TEOS was added dropwise. The reaction was continued at 80 °C for 2 h, after which the solution was cooled to room temperature and aged overnight.

Once nanoparticles precipitated, the solution was centrifuged at 4750 rpm for 10 min and the supernatant was removed. This process was repeated three times using water. The resulting MCM-41 was dried at 70 °C for about 12 hours. To remove the residual surfactant template, the dried MSNs were calcinated at 550 °C for 5 h, employing a heating rate of approximately 3 °C/min.

2.2.2. Gas Adsorption. We also measured gas adsorption properties, surface area, and pore size distribution of MCM-41. Measurements at pressures up to 1 bar were performed at 77 K and 300 K using a Micromeritics Gemini VII 2390 surface area analyzer. Before adsorption, powder samples were pretreated by applying heat, vacuum, and finally flowing gas to remove water and impurity gas molecules adsorbed in the pores. A small amount of sample (15−20 mg) was degassed under vacuum at 250 °C for at least 12 h in a Micromeritics Vac Prep 061 sample degas system. The Brunauer, Emmett, and Teller (BET) method was used to determine the specific surface area of the MCM-41 samples. The BET adsorption model implemented in the Micromeritics instrument software incorporates multilayer coverage. The pore size distribution was calculated using the Barrett−Joyner−Halenda (BJH) model, which is typically used for mesoporous materials.[24]

2.2.3. Differential Scanning Calorimetry and Thermogravimetric Analysis. To study the thermal stability of MCM-41, differential scanning calorimetry and thermogravimetry analysis (DSC/TGA) were conducted with a Setaran Setsys Evolution 1750 DSC/TGA analyzer. The sample and the reference crucibles were made from alumina. Samples were heated to 1500 °C at a rate of 10 °C/min and 50 °C/min. The carrier gas was air and the gas flow rate was 20 mL/min.

2.2.4. Powder X-ray Diffraction. We used a Scintag XRD diffractometer with Cu Kα to collect XRD powder patterns. XRD patterns were collected between 2θ angles from 1 to 10° with step size of 0.02° and scan rate 0.0012. Samples were mounted on zero-background holders. Measurements between 2θ angles from 20 to 60° were also made.

2.2.5. Heat Treatment. MCM-41 was treated at three different temperatures (500, 1000, and 1500 °C) to study thermal degradation. These temperatures were selected from the DSC/TGA results in section 3.1.3. MCM-41 was heated in the presence of air at 10 °C/min to the desired temperature using the Seteram Setsys Evolution 1750 DSC/TGA analyzer. The airflow rate was 20 mL/min. Once the sample achieved the desired temperature, the temperature was cooled at 20 °C/min to room temperature.

3. RESULTS AND DISCUSSION

We first present results drawn from pure simulation studies on MCM-41. Then the experimental measurements and comparisons to the predictions from simulations are described in details.

3.1. Molecular Dynamics Simulation. *3.1.1. The Degradation Process and Induced Morphology Change.* Figure 2a shows the simulated MCM-41 structure evolution during the heating process at a heating rate of 0.01 K/ps. The porous region maintains its regular interface until 2180 K, after which regularity quickly decreases along with roughening of the surface to a complete closure of the pores. If we take the temperature at which the porous region disappears as the collapse temperature, this value is found to vary with the heating rate as shown in Figure 2b. A faster heating rate results in a higher collapse temperature.

Systematic characterizations for the 300, 1273, 1773, 2415, 2180, 2650, and 2885 K models were performed to further understand the mechanism of porous structure evolution with temperature. The models that have been quenched to room temperature are first characterized by the radial density profile (Figure 2c).

The radial density profile shows the density change from the center of the pore to the matrix. The interface is defined as the range for which the density is larger than zero, but smaller than the bulk. Three changes with temperature were observed. First, the pore radius gradually decreases as the boundary of the silica matrix moves toward the pore center. If the pore radius is defined as the distance at which the density is half of the bulk, the untreated 300 K model has a radius around 13.5 Å, decreasing to ∼10 Å at 2650 K. Second, the slope which indicates the width of the interfacial range becomes less steep at higher temperatures. The original structure at 300 K has a steep density transition to the matrix, which means a very narrow interface and a well-defined surface. After heating, the surface

DOI: 10.1021/acs.langmuir.6b02814
Langmuir 2016, 32, 11422−11431

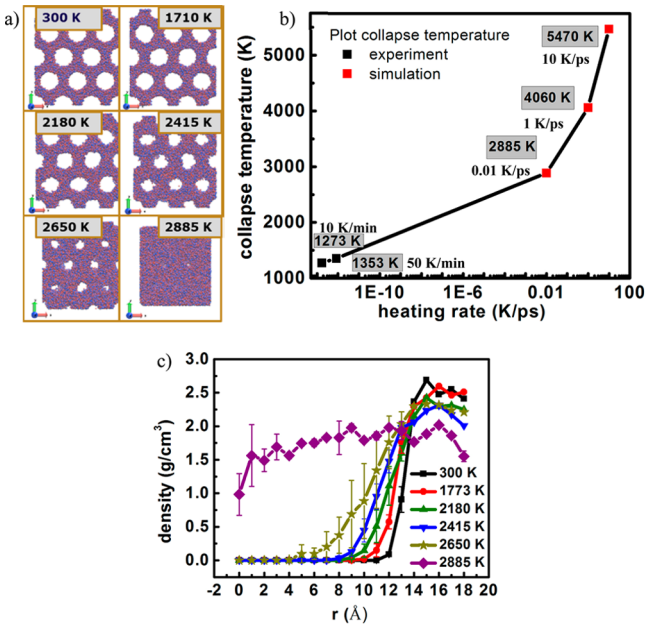

Figure 2. (a) MCM-41 structure snapshots during heating at heating rate of 0.01 K/ps of one amorphous cell. The output frequency of structure information is every 235 K. (b) MCM-41 structure's collapse temperature change with heating rate. Experiments used 10 and 50 K/min. Lines are a guide for the eye. (c) Radial density profile of the MCM-41 structure at different heating temperatures (averaged over all samples). The origin is chosen to be the center of the pore. Error bars are added for the interfacial region.

becomes rougher, as directly reflected by the surface contour (shown in Supporting Information, Figure S1).

The movement of the surface boundary and the increase of the interfacial width both indicate the diffusion of atoms toward the pore center, leading to the change of the matrix density (Table 2). We observe during the heat and quench stage that the cell volume also decreases. Up to 2415 K, the pore volume shrinkage is faster than the global volume change, so the matrix density first increases. This can be understood by the fact that at the beginning there is a large chemical potential gradient from the matrix to the pore region due to the surface energy and curvature of the pore. After diffusion the gradient becomes smaller and the matrix density change is dominated by the global volume shrinkage, as in the 2650 K case.

3.1.2. Discussion on the Mass Transfer Process. The mass transfer of the matrix atoms toward the porous region is found to occur more effectively during heating. During the hold stage at which the temperature is kept constant, the movement of surface boundary is not significant, though the movement becomes more pronounced with increasing temperature after 2180 K. This is apparent from a comparison of the radial density profile of structures at the beginning with that at the end of the hold stage (Supporting Information, Figure S2). Further diffusion characterization of oxygen and silicon atoms during the hold stage (Figure 3 and Table 3) show that two

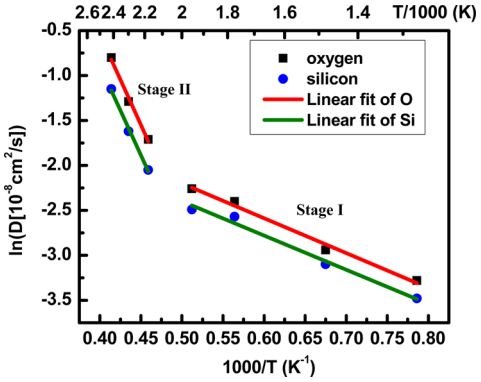

Figure 3. Arrhenius plot of diffusion coefficient versus temperature.

Table 3. Calculated E_a and D_0 for Both Oxygen and Silicon from Linear Fit of Figure 3

	oxygen stage I	oxygen stage II	silicon stage I	silicon stage II
D_0 (cm²/s)	0.75×10^{-8}	1.85×10^{-5}	0.61×10^{-8}	1.20×10^{-5}
E_a (kJ/mol)	34.1	167.6	31.6	165.9

mechanisms of diffusion exist. The first mechanism (stage I) has a relatively low activation energy and a low diffusion coefficient, while above 2180 K the second diffusion mechanism is triggered with an activation energy around 167 kJ/mol (stage II).

The latter value of 167 kJ/mol falls well within the range of previously found diffusion energy barriers in vitreous silica matrix, while the diffusion coefficient D_0 is much lower than that in bulk vitreous silica.[25] This may be due to the existence of the pore interface, which limits the atom's diffusion length to be within the matrix. As the kinetically related pore closure process happens mainly during heating, the activation energy needed for atoms to transfer from matrix to porous region must be higher than in the hold stage (at least below 2415 K) for a pure diffusion process. Previous studies[26] concluded that diffusion in the silica phase is a collective process that can involve different number of atoms leading to a continuous range of activation energies. The diffusion of the pore interface may involve almost all atoms, as the surface boundaries simultaneously move toward the porous region, thus requiring a higher activation energy. In terms of stage I, a low energy barrier usually results from annihilation/creation of one or two pairs of dangling bonds.[26] This is quite possible in MCM-41 due to the amorphous nature of the silica phase and the existence of surface dangling bonds.

The RDF calculated during the hold stage is presented in Figure 4 (averaged over the whole hold stage). For all three pairs (Si−O, O−O, and Si−Si), the position of the first dominant peak does not change, while the area below the peak decreases with temperature, indicating that the average coordination number decreases. This means that the diffusion of atoms from matrix to surface involves the breakage of many

Table 2. Matrix Density Change after Heat Treatment at Different Temperatures[a]

	300 K	1273 K	1773 K	2180 K	2415K	2650 K
ρ (g/cm³)	2.50 ± 0.11	2.47 ± 0.07	2.46 ± 0.08	2.29 ± 0.05	2.15 ± 0.03	2.28 ± 0.14

[a]The density is averaged over the data points starting from 14 Å for samples 1, 2, and 3. The standard deviation reflects the average density deviation among the three samples.

DOI: 10.1021/acs.langmuir.6b02814
Langmuir 2016, 32, 11422−11431

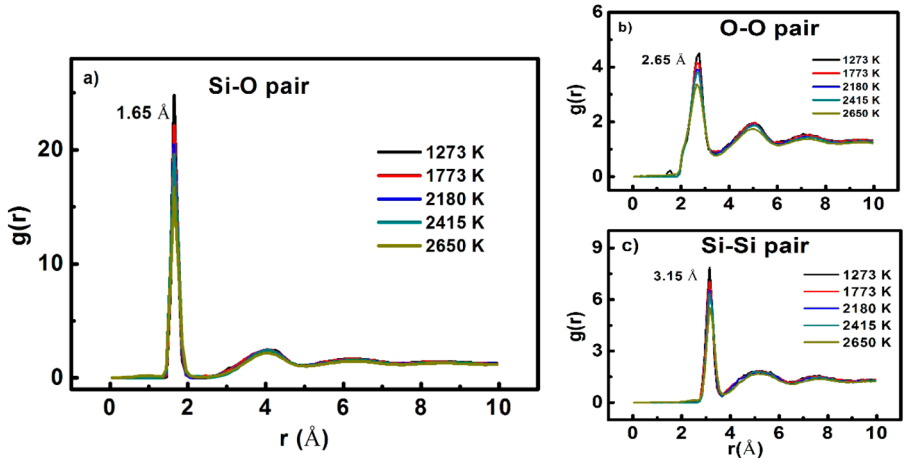

Figure 4. Radial distribution function of MCM-41 obtained during holding stage for different temperatures.

Table 4. Coordination Number (CN) Characterization of Oxygen Atoms at the Surface of MCM-41 Structure Heated to Different Temperature

	300 K	1273 K	1773 K	2180 K	2415 K	2650 K
radius (Å)	13.7	13.5	13	12	11	10
total surface O	51 ± 8	52 ± 1	60 ± 13	53 ± 26	38 ± 16	56 ± 9
CN = 1 O number	31 ± 6	23 ± 2	9 ± 2	3 ± 2	2 ± 0	1 ± 0

Si−O bonds, possibly to create large number of vacancies and interstitials for diffusion; bonds then reform at the pore surface. Notice that, although the RDF is characterized during the hold stage, this matrix-to-pore surface diffusion mainly occurs during the heating stage as discussed previously.

To verify bond reformation, the number of oxygen dangling bonds at the surface is calculated (Table 4). Since the pore radius also decreases during heat treatment the surface region is redefined for every sampled temperature; this keeps the total number of oxygen atoms within that region constant (radius value in Table 4). A dangling bond in an oxygen atom is reflected by a coordination number (CN) of one. The cutoff for CN is chosen to be 2.0 Å, which is slightly larger than the Si−O bond length. As shown in Table 4, the undercoordinated (CN = 1) oxygens decrease significantly during thermal degradation, indicating the reformation process happens during heating treatment. Since dangling bonds lead to higher surface energy, it is reasonable that the system will tend to reduce the number of dangling bonds and move to a more energetically favorable structure: a homogeneous matrix phase without pores. The configuration of the three samples for the 2650 K model has a larger deviation relative to the configuration at other temperatures, so the radius defining the surface area here is the average value of the three samples. For models at other temperatures, the radius is identical for all three samples.

3.1.3. Discussion on the Accuracy of the Model Compared to Experiments. For the simulated thermal degradation process we seek to determine how closely simulation reflects real structures and processes in MCM-41. The originally built 300 K model correctly represents the characteristic RDF, bond angle distribution and coordination number of amorphous silica phase (Supporting Information, Figure S3 and Table S1). When deleting atoms to create the porous region, the surface is left with oxygen and silicon dangling bonds. No hydrogen atoms are attached since this model is fully dehydroxylated to avoid water formation during heating (the Tersoff potential used here allows the change of bond strengths according to coordination numbers, and thus bond formation and breakage can be allowed and characterized with coordination number change). This differs from the experimental case, since silanol groups (Si−O−H) would be present after the sol−gel synthesis process. The unsaturated silicon and oxygen bonds in our model may lead to a different surface energy and bond reformation process. The dehydroxylation of amorphous silica surface −OH groups happens at 190−900 °C,[27] such that dehydroxylation completes before structure degradation (around 1000 °C, as shown later in our experiments). Thus, the absence of silanol groups should not affect the thermal degradation process. The unsaturated oxygen and silicon atom numbers in our model are used to determine the dangling bond density (see Table 5). The experimental density of surface

Table 5. Dangling Bond Density at the Pore Surface[a]

dangling bond type	unsaturated O (−Si)	unsaturated Si (−O)	total value
density (#/nm^2)	3.3	1.8	5.1

[a]The element in parentheses shows the connected atom type.

dangling bonds (characterized by the hydroxyl group concentration) is between 4.5 and 6.2/nm^2. For comparison, previous simulations by others predict a density in the range 3.9−8.4/nm^2.[28] The dangling bond density obtained here (5.1/nm^2) falls well within the accepted range.

Second, we note that the temperature scale obtained in the simulation is much higher than in experiments due to the extremely fast heating rate in the simulation. In experiments, the porous structure is found to collapse around 1273 K, as revealed from XRD and gas adsorption measurement (Figure 5). This result is consistent with previous studies.[6] The three peaks present in the untreated original sample reflect the hexagonal arrangement of pores, and they gradually disappear after heat treatment. This behavior could either be due to the loss of periodicity in the porous structure, the increase of

DOI: 10.1021/acs.langmuir.6b02814
Langmuir 2016, 32, 11422−11431

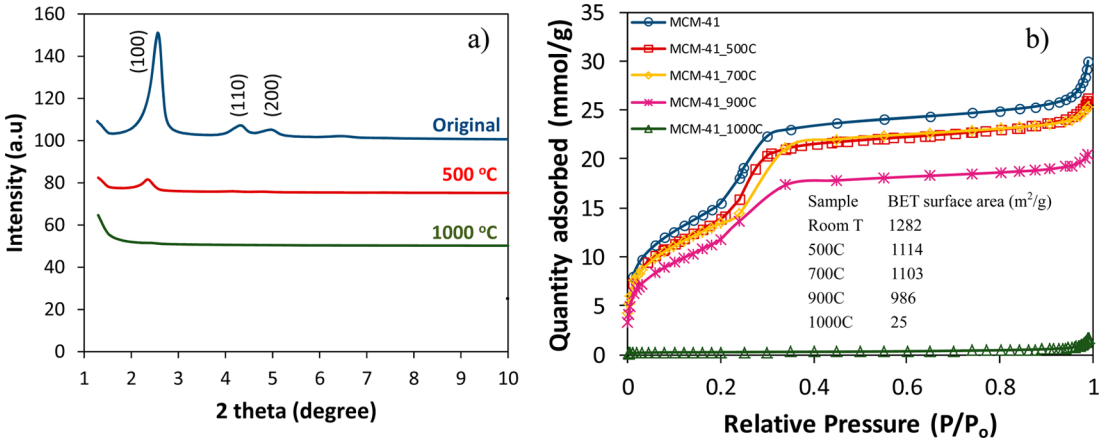

Figure 5. (a) XRD patterns of heated MCM-41 samples compared with the untreated sample (original) at room temperature. (b) Nitrogen adsorption isotherms at 77 K for the untreated MCM-41 and MCM-41 heated to 500, 700, 900, and 1000 °C. Values for the BET surface areas are given in the figure.

irregularity of the pore surface, the change of the pore size distribution, the disappearance of the pores, or some combination of these influences. The BET surface area based on the gas adsorption measurements supports the decrease and collapse of the porous region with increasing temperature.

This heating rate effect is well-known in differential thermal analysis.[29,30] In any reaction with an activation energy, the endothermal/exothermal peak position will vary with the heating rate. Kissinger proposed an equation, eq 4, to calculate the activation energy for the reaction based on the heating rate:[29]

$$\frac{d\left(\ln \frac{\beta}{T_p^2}\right)}{d\left(\frac{1}{T_p}\right)} = -\frac{E_A}{R} \tag{4}$$

where β is the heating rate, T_p is the temperature at the heat flow peak, E_A is the activation energy, and R is the gas constant.

As noted previously, pore closure is a thermally activated process. In our study, T_p is the collapse temperature shown in Figure 2b at different heating rates. TG/DSC analysis in experiments shows a similar peak around 1273 K (Supporting Information, Figure S4). By applying the left side of eq 4 to the collapse temperature T_p and heating rate β, a linear correlation is obtained between simulation and experimental data points (Figure 6). This indicates that the change of the collapse temperature with heating rate is well-described by Kissinger's equation: the pore-closure process needs activation energy and is kinetically dependent. Moreover, it implies the consistency between the simulated and the experimental degradation process in that they have the same activation energy. With the validation of eq 4 for our case, the collapse temperature at other heating rates can also be predicted. This method can be extended to other simulation cases to attain the value for the experimental case. The activation energy for complete pore closure is found to be 416 ± 17 kJ/mol from the linearly fitted slope value in Figure 6 (which represents $-\frac{E_A}{R}$), and the error value comes from the standard error of fitting. Given the Si−O bond breaking energy of 452 kJ/mol,[31] the obtained activation energy is at the same order and thus bond breaking is likely to be the bottleneck process for pore closure. Meanwhile, the simulated activation energy for self-diffusion in vitreous silica of

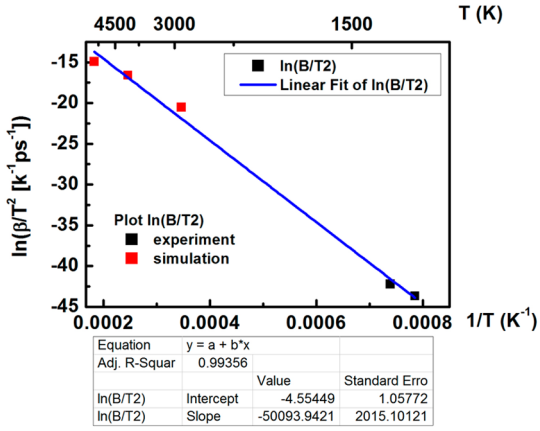

Figure 6. Linear fit to obtain activation energy using Kissinger equation.

oxygen and of silicon each is around 168 kJ/mol. If simultaneous diffusion of these two types of atoms happens during pore closure process, the total activation energy for collective diffusion is around 336 kJ/mol, which is smaller than the pore closure energy barrier. Therefore, the value obtained for the activation energy for complete pore closure justifies a possible pore closure process involving both bond dissociation and atom's diffusion, as concluded from mass transfer process discussion.)

Some deficiencies exist in the simulation model due to the periodic boundary condition compared to the experimental case. For example, thermal treatment above 1000 °C in experiments will convert amorphous silica to a cristobalite phase (detected at 1500 °C, Supporting Information, Figure S5), while in the simulation this phase transition is not observed. This is due to the restriction of the unit cell size used for MCM-41 structure, as the periodic boundary condition requires an integer number of unit cells of cristobalite within the MCM-41 unit cell, however this cannot be the case here. And the crystallization at this simulation scale can be very slow. Also, there is no pore size distribution included in our model. It is possible that pore curvature influences the kinetic degradation process, for example such that smaller pores close faster than larger pores.

DOI: 10.1021/acs.langmuir.6b02814
Langmuir 2016, 32, 11422−11431

Based on previous studies, we conclude that the pore closure process is kinetically dependent and requires an activation energy of about 416 kJ/mol. This energy indicates the bond breakage likely to be the bottleneck process in pore closure, accompanied by diffusion of oxygen and silicon atoms (the simultaneous diffusion of these two types of atoms is also allowed) and bond reformation at pore surface. Although the model is not able to capture crystallization and pore size distribution, it does show a consistent trend with experiments and provides a reasonable pore collapse mechanism. In the next section, one of the thermally treated models along with the 300 K model will be simulated to predict and compare their gas adsorption and selectivity properties.

3.2. Gas Adsorption and Selectivity Studies. We choose the 300 K (d = 28 Å) and the 2650 K model from the previous thermal degradation simulation for additional study. Adsorption behavior is compared in the 1−10 000 kPa range at room temperature. The 2650 K model is selected because this stage can show significant morphological changes while still keeping the porous structure.

3.2.1. Discussion on the Accuracy of the Model. The comparison between simulation and experimental N_2 adsorption data are provided at 77 and 300 K, as shown in Figure 7.

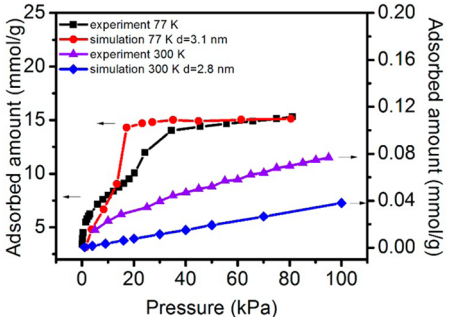

Figure 7. Simulated N_2 adsorption at 77 and 300 K compared to experiments. The 300 K MCM-41 models of diameters = 2.8 and 3.1 nm were used.

The adsorption quantity is obtained without normalization and the models qualitatively produce the expected adsorption isotherms. The simulation models are simplified without silanol groups (no hydrogen atoms are attached to dangling oxygen), because Lennard−Jones parameters for hydrogen are negligible compared those for to oxygen,[11] and adsorbates here (N_2, Ar, Kr, and Xe) are nonpolar and will not be influenced by Coulomb interaction introduced with silanols. The surface roughness modification by attaching hydrogen atoms is also limited comparing to that modified by thermal treatment: the OH distance is less than 1 Å, while thermal treatment can lead to several angstroms' surface change (Figure 2). Experimental average pore diameter evaluated by geometrical model is 3.4 nm, which is slightly larger than our simulation models following $r_p(g) = a_0\sqrt{\frac{\sqrt{3}}{2\pi}\left(\frac{\rho_{sil}V_p}{1+\rho_{sil}V_p}\right)}$ according to ref 32, where a_0 is the unit cell parameter obtained from XRD, ρ_{sil} the density of the silica, and V_p the pore volume. This model has also been shown to agree well with DFT calculations.[32] The silica skeleton's density in our model reaches 2.5 g/cm^3 after NPT equilibration, while in most simulation cases the density value of 2.2 g/cm^3 is used. Better estimates of these parameters would enable a more accurate model. Nevertheless, since this study focuses on the comparison of models under different heat treatment the model quality is sufficient.

3.2.2. Single Component Adsorption Behavior. Single component adsorption was studied to compare the two MCM-41 models (with and without heat treatment) at room temperature (300 K) over a wide pressure range (Figure 8). For N_2, Ar, and Kr, adsorption changes from the gas phase to the supercritical phase far away from the critical point with increase of pressure. The storage quantity first shows a linear relation in the low pressure region (Figure 8c−f, the N_2 results agree with literature[11]). It reflects a typical Henry's adsorption isotherm whose slope is proportional to Henry's constant K_H. The adsorption then gradually deviates from linearity and tends toward saturation with increasing pressure. For the 300 K model this is mostly due to the intrinsic density saturation of supercritical gas, while for the 2650 K model, since the deviation happens at an earlier stage, it indicates the interaction between adsorbate and adsorbent becomes stronger. The saturation amount clearly drops in the 2650 K model compared to the 300 K model, confirming a decrease of pore volume after heat treatment. For Xe, 300 K is close to its critical point (289.8 K, 57.6 atm) and the density increase from the gas phase to the supercritical phase is much steeper. As a result, the storage isotherm shows a condensation-like process around 3000 kPa for the 300 K model. For the 2650 K model, the Xe storage quantity changes to a micropore-filling behavior because the pore size is smaller.

Interestingly, if the 300 K model is compared to the 2650 K model in the low pressure region (0−100 KPa, Figure 8c−f), the change of the storage quantity for different adsorbates does not show the same trend. For example, for N_2 and Ar (Figure 8c and d), the values decrease in the 2650 K model; while for Kr and Xe (Figure 8e and f), the storage amount increases.

3.2.3. Gas Mixture Behavior. It is also important to understand how selectivity changes with heat treatment. Binary gas mixture adsorption simulation were performed for Kr/Xe and Kr/Ar. The selectivity S_{xy} is defined as

$$S_{xy} = \frac{x_i y_j}{x_j y_i} \tag{5}$$

where i, j denote the atom types, x is the amount of different molecular types in free space, and y is absolute adsorbed amount. Figure 9a shows the Kr/Ar selectivity with and without heat treatment. For the 300 K model selectivity first decreases with pressure and then stays constant after 5000 kPa as the adsorption difference of the two adsorbates due to their interaction energy keeps decreasing with this pressure and eventually flattens out as at high pressures selectivity is mainly defined by the supercritical phase density ratio.

For the 2650 K model, selectivity is increased, especially for the low-pressure region (0−100 kPa). From single component adsorption we know that the interaction energy of larger molecules increases faster as a function of pressure increasing selectivity. Eventually, when the pressure is high enough (around 100 bar), selectivity is mainly defined by the ratio of the supercritical phase quantities. At this point, the selectivity of different models converge. For the Xe/Kr case (Figure 9b), similarly the selectivity of the 2650 K model is higher than the 300 K model. The small peak around 5000 kPa in both models is probably due to the steep increase of Xe density around that pressure, leading to an immediate saturation of Xe. Then Kr also begins to saturate and the selectivity gradually decreases.

DOI: 10.1021/acs.langmuir.6b02814
Langmuir 2016, 32, 11422−11431

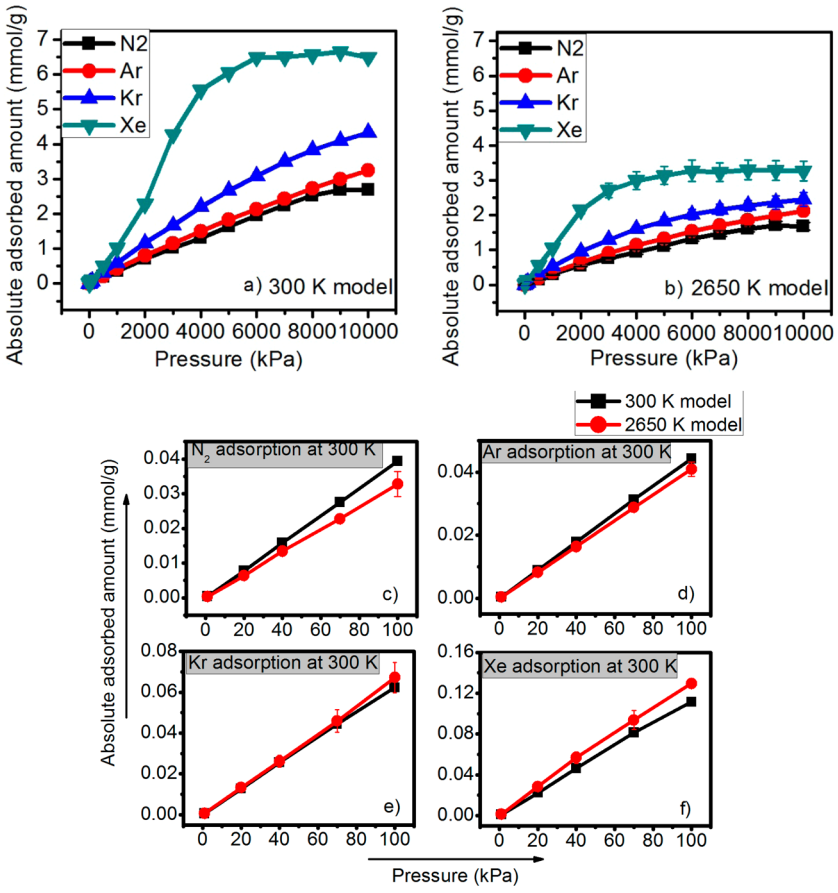

Figure 8. Simulated adsorption isotherms of different gases at 300 K by (a) 300 K MCM-41 model and (b) 2650 K MCM-41 model. (c–f) Comparison of the 300 K model adsorption with the 2650 K model adsorption for the 1–100 kPa range. For the 2650 K model, the results are averaged over three samples. Error bars that are not visible are smaller than data points.

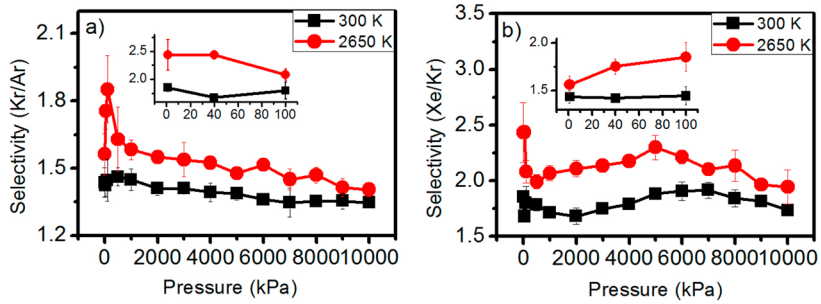

Figure 9. (a) Kr/Ar selectivity and (b) Xe/Kr selectivity comparison between 300 K model and 2650 K model. Insets are zoomed-in from 0 to 100 kPa.

4. CONCLUSION

Molecular dynamics simulations of MCM-41 reveal that the porous structure gradually closes during heating and eventually disappears at a critical temperature that depends on the heating rate. By applying the Kissinger equation, a strong correlation between simulated pore collapse temperature and experimental values is established. We calculate an activation energy of 416 ± 17 kJ/mol for the pore closure reaction. In simulations we calculate the radial density profile (RDF) and oxygen dangling bonds. The temperature-dependent evolution of these quantities indicates that silicon and oxygen atoms move from the silica matrix to the pore surface to close the pore. This process likely requires a collective diffusion of most matrix atoms toward the pore region, the breakage of Si–O bonds in the matrix and a bond reformation at the surface.

Monte Carlo simulations illustrate the adsorption behavior of typical MCM-41 type structures at 300 K over a pressure range from 1 to 10000 kPa for N_2 and different noble gases. The absolute adsorption quantity of N_2, Ar and Kr increases linearly with pressure, then saturates gradually. For Xe, a steep increase in adsorption around 3000 kPa is likely due to its intrinsic density jump from gas phase to supercritical phase. The decrease of the average pore size and the increase of surface roughness of the 2650 K model leads to a stronger adsorption energy by a curvature effect, while the decrease of pore volume leads to a contradictory modification on the absolute adsorption amount. The impact of these two factors varies

DOI: 10.1021/acs.langmuir.6b02814
Langmuir 2016, 32, 11422–11431

for small and large molecules. The absolute adsorption quantity of N_2 and Ar decreased in the 2650 K model, while that of Kr and Xe increased. This effect leads to increased selectivity for the Kr/Ar and Xe/Kr gas pairs.

Based on these results, we conclude that thermal treatment may increase the selectivity between noble gases for appropriate temperatures. Selectivity could be extended to other type of adsorbates, such as H_2O, CO_2, and alkane gases. We anticipate that the selectivity modification by thermal treatment for these gases will become more significant, since their adsorption energy can differ significantly due to electrostatic interactions (dipole for H_2O, quadrupole for CO_2, etc.). Future studies could examine other porous materials that undergo surface boundary diffusion while the surface energy is also modified during heat treatment, with potential application to catalysis and other scientifically and industrially relevant processes.

■ ASSOCIATED CONTENT

Supporting Information

The Supporting Information is available free of charge on the ACS Publications website at DOI: 10.1021/acs.langmuir.6b02814.

Comparison of surface roughness; radial density profiles; coordination numbers for Si and O atoms in bulk; DSC/TG profiles; XRD pattern (PDF)

■ AUTHOR INFORMATION

Corresponding Authors

*E-mail: rfaller@ucdavis.edu.

*E-mail: pstroeve@ucdavis.edu.

Notes

The authors declare no competing financial interest.

■ ACKNOWLEDGMENTS

This work was supported by the U.S. Department of Energy Nuclear Energy University program under Grant DE-NE0000704. Some parts of this work were performed under the auspices of the U.S. Department of Energy by Lawrence Livermore National Laboratory under Contract DE-AC52-07NA27344. Lawrence Livermore National Security, LLC.

■ REFERENCES

(1) Cruciani, G. Zeolites upon heating: Factors governing their thermal stability and structural changes. *J. Phys. Chem. Solids* **2006**, *67*, 1973−1994.

(2) Borchardt, L.; Hoffmann, C.; Oschatz, M.; Mammitzsch, L.; Petasch, U.; Herrmann, M.; Kaskel, S. Preparation and application of cellular and nanoporous carbides. *Chem. Soc. Rev.* **2012**, *41*, 5053−5067.

(3) Chen, C.-Y.; Li, H.-X.; Davis, M. E. Studies on mesoporous materials: I. Synthesis and characterization of MCM-41. *Microporous Mater.* **1993**, *2*, 17−26.

(4) Chen, L. Y.; Jaenicke, S.; Chuah, G. K. Thermal and hydrothermal stability of framework-substituted MCM-41 mesoporous materials. *Microporous Mater.* **1997**, *12*, 323−330.

(5) Tompkins, J. T.; Mokaya, R. Steam Stable Mesoporous Silica MCM-41 Stabilized by Trace Amounts of Al. *ACS Appl. Mater. Interfaces* **2014**, *6*, 1902−1908.

(6) Chen, H.; Wang, Y. Preparation of MCM-41 with high thermal stability and complementary textural porosity. *Ceram. Int.* **2002**, *28*, 541−547.

(7) Maddox, M. W.; Olivier, J. P.; Gubbins, K. E. Characterization of MCM-41 Using Molecular Simulation: Heterogeneity Effects. *Langmuir* **1997**, *13*, 1737−1745.

(8) He, Y.; Seaton, N. A. Experimental and computer simulation studies of the adsorption of ethane, carbon dioxide, and their binary mixtures in MCM-41. *Langmuir* **2003**, *19*, 10132−10138.

(9) Coasne, B.; Hung, F. R.; Pellenq, R. J. M.; Siperstein, F. R.; Gubbins, K. E. Adsorption of sample gases in MCM-41 materials: The role of surface roughness. *Langmuir* **2006**, *22*, 194−202.

(10) Hung, F. R.; Bhattacharya, S.; Coasne, B.; Thommes, M.; Gubbins, K. E. Argon and krypton adsorption on templated mesoporous silicas: molecular simulation and experiment. *Adsorption* **2007**, *13*, 425−437.

(11) Chang, S.-C.; Chien, S.-Y.; Chen, C.-L.; Chen, C. o.-K. Analyzing adsorption characteristics of CO2, N2 and H2O in MCM-41 silica by molecular simulation. *Appl. Surf. Sci.* **2015**, *331*, 225−233.

(12) Huang, L.; Kieffer, J. Molecular dynamics study of cristobalite silica using a charge transfer three-body potential: Phase transformation and structural disorder. *J. Chem. Phys.* **2003**, *118*, 1487−1498.

(13) Palace Carvalho, A. J.; Ferreira, T.; Estêvão Candeias, A. J.; Prates Ramalho, J. P. Molecular simulations of nitrogen adsorption in pure silica MCM-41 materials. *J. Mol. Struct.: THEOCHEM* **2005**, *729*, 65−69.

(14) Nichols, J.; Binford, F. *Status of Noble Gas Removal and Disposal*; Oak Ridge National Laboratory: Oak Ridge, TN,1971.

(15) Sha, H.; Faller, R. Molecular simulation of adsorption and separation of pure noble gases and noble gas mixtures on single wall carbon nanotubes. *Comput. Mater. Sci.* **2016**, *114*, 160−166.

(16) Sha, H.; Faller, R. A quantum chemistry study of curvature effects on boron nitride nanotubes/nanosheets for gas adsorption. *Phys. Chem. Chem. Phys.* **2016**, *18*, 19944−19949.

(17) Plimpton, S. Fast parallel algorithms for short-range molecular dynamics. *J. Comput. Phys.* **1995**, *117*, 1−19.

(18) Tersoff, J. New empirical approach for the structure and energy of covalent systems. *Phys. Rev. B: Condens. Matter Mater. Phys.* **1988**, *37*, 6991.

(19) Munetoh, S.; Motooka, T.; Moriguchi, K.; Shintani, A. Interatomic potential for Si−O systems using Tersoff parameterization. *Comput. Mater. Sci.* **2007**, *39*, 334−339.

(20) Martin, M. G. MCCCS Towhee: a tool for Monte Carlo molecular simulation. *Mol. Simul.* **2013**, *39*, 1212−1222.

(21) Waldman, M.; Hagler, A. New combining rules for rare gas van der Waals parameters. *J. Comput. Chem.* **1993**, *14*, 1077−1084.

(22) Bezus, A. G.; Kiselev, A. V.; Lopatkin, A. A.; Du, P. Q. Molecular statistical calculation of the thermodynamic adsorption characteristics of zeolites using the atom−atom approximation. Part 1.—Adsorption of methane by zeolite NaX. *J. Chem. Soc., Faraday Trans. 2* **1978**, *74*, 367−379.

(23) Yang, J.; Ren, Y.; Tian, A.-m.; Sun, H. COMPASS force field for 14 inorganic molecules, He, Ne, Ar, Kr, Xe, H2, O2, N2, NO, CO, CO2, NO2, CS2, and SO2, in liquid phases. *J. Phys. Chem. B* **2000**, *104*, 4951−4957.

(24) Storck, S.; Bretinger, H.; Maier, W. F. Characterization of micro- and mesoporous solids by physisorption methods and pore-size analysis. *Appl. Catal., A* **1998**, *174*, 137−146.

(25) Litton, D. A.; Garofalini, S. H. Vitreous silica bulk and surface self-diffusion analysis by molecular dynamics. *J. Non-Cryst. Solids* **1997**, *217*, 250−263.

(26) Mousseau, N.; Barkema, G. T.; de Leeuw, S. W. Elementary mechanisms governing the dynamics of silica. *J. Chem. Phys.* **2000**, *112*, 960−964.

(27) Zhuravlev, L. The surface chemistry of amorphous silica. Zhuravlev model. *Colloids Surf., A* **2000**, *173*, 1−38.

(28) Feuston, B.; Higgins, J. Model structures for MCM-41 materials: a molecular dynamics simulation. *J. Phys. Chem.* **1994**, *98*, 4459−4462.

(29) Kissinger, H. E. Reaction Kinetics in Differential Thermal Analysis. *Anal. Chem.* **1957**, *29*, 1702−1706.

(30) Kissinger, H. E. Variation of peak temperature with heating rate in differential thermal analysis. *J. Res. Natl. Bur. Stand* **1956**, *57*, 217.

(31) Zumdahl, S. S. *Chemistry*, 5th ed.; Brooks Cole: Pacific Grove, CA, 1999; p 373, Table 8.4.

DOI: 10.1021/acs.langmuir.6b02814
Langmuir 2016, 32, 11422−11431

(32) Ribeiro Carrott, M.; Candeias, A. E.; Carrott, P. J. M.; Ravikovitch, P. I.; Neimark, A. V.; Sequeira, A. D. Adsorption of nitrogen, neopentane, n-hexane, benzene and methanol for the evaluation of pore sizes in silica grades of MCM-41. *Microporous Mesoporous Mater.* **2001**, *47*, 323−337.

DOI: 10.1021/acs.langmuir.6b02814
Langmuir 2016, 32, 11422−11431